

## LABORATORY STUDY OF THE DYNAMICS OF JOVIAN-TYPE VORTICES

S.D. MEYERS, J. SOMMERIA\* and Harry L. SWINNEY

*Department of Physics and the Center for Nonlinear Dynamics, University of Texas, Austin, TX 78712, USA*

A laboratory experiment on a turbulent shear flow in a rapidly rotating annulus yields vortices with many properties of jovian vortices, including their spontaneous formation and persistence, the merger of vortices of like sign, and particle trapping. When the fluid is strongly forced (Reynolds number  $\geq 10^4$ ), a wide zone of nearly uniform potential vorticity forms, and vortices successively merge until only a single dominant vortex remains. In the less turbulent flow of a weakly forced fluid, the zone of uniform potential vorticity is narrower and multiple vortex states are found. These observations are compared to numerical simulations and to related experiments as well as to jovian vortices.

### 1. Introduction

More than three centuries ago Hooke [1] reported the observation of a “spot in the biggest of the three obscurer belts of Jupiter”; this presumably was the first sighting of the Great Red Spot (GRS). Subsequent terrestrial observations revealed other persistent spots, but the most detailed picture of the jovian atmosphere has been provided by the two Voyager spacecraft, each of which observed Jupiter for about two months in 1979. The Voyager data show that:

(i) Persistent vortices are common. More than 100 spots were observed in the zonal flows that roughly alternate direction with latitude; see fig. 1. Spots occur in both wide zones and narrow zones and in both the northern and southern hemispheres (the GRS is centered at  $22.5^\circ$  S). The spots vary in size from 25 000 km (the GRS) down to less than 500 km. The majority of the observed spots lasted for the full duration of the observations.

(ii) When spots interact, they usually merge (24 mergers were observed for the 27 observed pairs of interacting spots) [2].

(iii) Some latitudinal zones, including the one containing the Great Red Spot, appear strongly turbulent (see fig. 1). They exhibit a large shear with the zonally averaged velocity varying in some cases by 100 m/s over a few degrees in latitude, yet the zonally averaged velocity profiles are very stable – the velocity profiles determined at a five month interval by Voyagers 1 and 2 were 99.8% correlated [3].

The stability of vortices in conditions that would normally inhibit the existence of long-lived coherent structures is a vexing problem in fluid mechanics, one addressed by the present study. Although no single experiment can hope to capture all the complex dynamics present in a planetary atmosphere, we find that many of the characteristics of the GRS and other jovian vortices are described by a simple barotropic model. Numerical simulation on this barotropic model [4] and our experiments, taken together, provide a reasonable description of the basic dynamics of the GRS.

Our observations of persistent vortices were reported previously in a brief letter [5]; also, using the same apparatus we have conducted complementary experiments on Rossby waves in eastward jets [6, 7]. Here we report new experiments that examine the robustness of the vortices, the

\*Permanent address: Madydam, ENSHMG, BP 95, 38402 St. Martin D’Heres Cedex, France.

role of potential vorticity, the dynamics of the merging process and particle transport.

The apparatus and the generation of strong westward jets is described in section 2. The basic results on the formation of vortices in a turbulent shear flow are presented in section 3, and our observations are discussed and compared with the observations for Jupiter, numerical simulations, and other experiments in section 4.

## 2. Experiment

### 2.1. Apparatus

The rigid rotating annulus, shown in fig. 2, has been designed to generate a fluid flow that mimics in a simple way the conditions found in the jovian atmosphere [5, 6]. Several previous experiments, some of which are described in section 4.5, have successfully captured different aspects of planetary flows. Our system is designed to produce a strongly turbulent (though essentially two-dimensional) weakly dissipative shear flow, as occurs between the strong eastward and westward jets on Jupiter. In our experiment a westward jet is produced by the action of the Coriolis force on fluid pumped continuously radially outward from a ring of sources to a ring of sinks. The rotation rate is large (up to 4 Hz) so that the Ekman number is small, typically  $\sim 10^{-6}$ , and the Rossby number is only about 0.1 (the Rossby number for the GRS is about 0.2). The Reynolds number ranges up to about  $2 \times 10^5$ , well into the turbulent domain.

For an inviscid flow in the limit of zero Rossby number (a *geostrophic* flow) there is no variation in the velocity in the direction parallel to the rotation vector. Therefore, a fluid with horizontal boundaries would have no velocity component in the vertical direction – the flow would be purely two-dimensional. For small Rossby number vertical variations in fluid velocity are on the order of the Rossby number. In a viscous fluid, departures from geostrophy occur primarily in the upper and lower Ekman boundary layers, which can inject

fluid vertically into low pressure regions and withdraw fluid from high pressure regions; this Ekman pumping drives a weak ageostrophic recirculation within each vortex. The effect of the Coriolis force on this recirculating motion is called the Ekman friction.

The vorticity equation for a single uniform layer of fluid in geostrophic motion expresses the conservation of *potential vorticity*,

$$q = (\omega + 2\Omega \sin \phi)/h, \quad (1)$$

$$[\partial/\partial t + (\mathbf{u} \cdot \nabla)]q = 0, \quad (2)$$

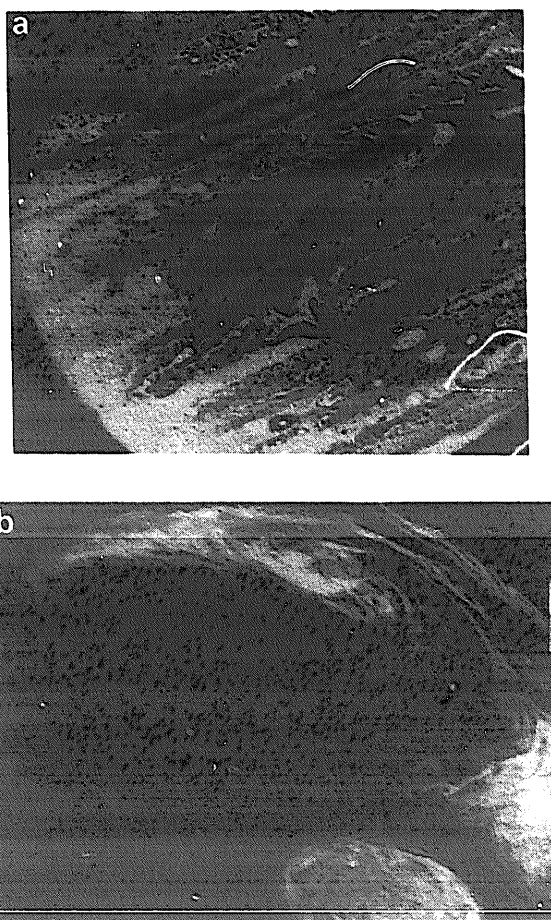


Fig. 1. (a) This composite photograph from Voyager 1 shows the turbulent zonal flow on Jupiter. Jovian vortices are clearly separated from the background flow, in spite of the surrounding turbulence. (b) The Great Red Spot and the smaller White Oval in the lower right each have a velocity minimum in the vortex center, as might be expected for vortices that are larger than the deformation radius. (Photographs from Jet Propulsion Laboratory, NASA.)

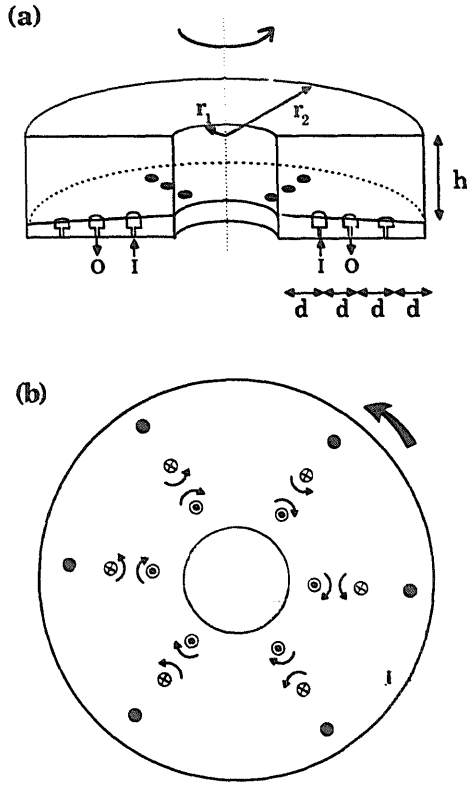


Fig. 2. (a) A cross section of the tank used to conduct the experiments is shown [5, 6]. The working basin has an inner diameter of 21.6 cm and an outer diameter of 86.4 cm. The depth increases from 17.1 cm at the inner radius to 20.3 cm at the outer radius; thus the conical bottom has a slope of  $-0.1$ . Fluid is pumped through the ports in the bottom in a variety of patterns, yielding different flow states; arrows indicate the pattern of inlets (I) and outlets (O) used in most of the present experiments. (b) The flow pattern immediately after starting the pump consists of anticyclonic vortices above each inlet and cyclonic vortices above each outlet; however, except at very low flow rates, this flow is unstable and a strong azimuthal jet develops.

where  $\omega$  is the relative vorticity,  $\Omega$  is the rotation rate,  $h$  is the fluid depth,  $\phi$  corresponds to planetary latitude, and  $\partial/\partial t + (\mathbf{u} \cdot \nabla)$  is the material derivative. Since the flow is quasi-two-dimensional, the potential vorticity is approximately conserved for each fluid column. For a narrow region about a fixed latitude  $\phi_0$  of constant depth  $h_0$  the potential vorticity can be approximated by expanding  $\sin \phi$  in a Taylor series about  $\phi_0$ ; this yields  $q \cong (\omega + 2\Omega(\sin \phi_0) + \beta y)/h_0$ , where  $\beta = 2\Omega(\cos \phi_0)/R$ ,  $y$  is the latitudinal displacement, and  $R$  is the radius of the planet.

In our experiment the variation of the Coriolis force with latitude in a planetary atmosphere, the *beta effect* [8], is mimicked to first order in the rotating annulus by a conical bottom (the upper lid is flat). The fluid depth can then be written  $h = h_0 - sr$ , where  $s$  is the slope of the bottom ( $s = -0.1$  in our annulus). If  $|sr| \ll h_0$  then eq. (1) becomes (with  $\phi_0 = \pi/2$ )  $q \cong (\omega + 2\Omega + \beta r)/h_0$ , where  $\beta = 2\Omega s/h_0$ ; this is the same expression for  $q$  as in a barotropic atmosphere, given in the previous paragraph. Dropping the constant term  $2\Omega$  and absorbing the constant factor  $h_0$  into  $q$ , we have

$$q = \omega + \beta r. \quad (3)$$

Actually, the conical bottom in our experiment does not produce a true beta effect in the original sense of latitudinally independent planetary vorticity. This can be seen by examining the potential vorticity equation, as discussed by Pedlosky [8] (see his eq. (3.15.1)): the term  $(\partial p/\partial x)\beta$  on the beta-plane becomes  $(\partial p/\partial \theta)\beta/r$  on the beta-annulus (where  $p$  is the pressure). If the dynamics of the flow are to remain unchanged in going from the beta-plane to the beta-annulus, then  $\beta$  must be a linear function of  $r$  (i.e., the annulus would need quadratic topography) and not a constant as (3) assumes. However, a constant beta is a good first order approximation to a true beta effect, and the flows we generate have many of the properties of large-scale planetary flows [5–7] in spite of our linear topography.

## 2.2. Azimuthal jet with uniform potential vorticity

When the pump is first activated, vortices form over the active ports, as represented in fig. 2(b). For low total pumping rates  $F$  (less than about  $20 \text{ cm}^3/\text{s}$ ) each source or sink produces a vortex that stays in the neighborhood of a port, with sinks producing cyclonic vortices and sources producing anticyclonic vortices. However, for larger pumping rates this flow is unstable and the vortices are advected eastward, resulting in a continuous jet.

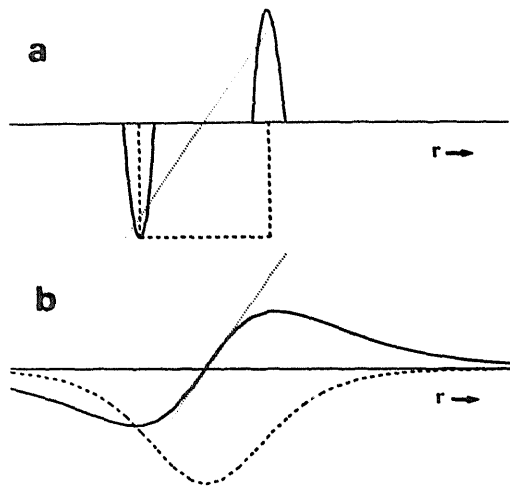


Fig. 3. The generation of a westward jet is indicated schematically. Dashed lines represent velocity, solid lines represent vorticity, and dotted lines correspond to vorticity with slope equal to  $|\beta|$ , signifying marginal stability. (a) When the pump is first activated, strong vortices form over the ports, but the stability of this flow is not assured by the Rayleigh-Kuo condition. (b) The flow evolves until the vorticity profile achieves marginal stability,  $(\partial\omega/\partial r)_{\max} = |\beta|$ .

The jet broadens until it satisfies the Rayleigh-Kuo stability condition for geostrophic motion [9]: the derivative of the potential vorticity  $\partial q/\partial r$  does not change sign. (Here we have substituted  $dq/dr$  for  $dq/dy$ , again neglecting the curvature of the annulus.) Marginal stability is achieved when  $\partial q/\partial r = 0$  somewhere in the flow, but there is still no change of sign. The marginal stability condition can be rewritten  $(\partial\omega/\partial r)_{\max} = |\beta|$ , which is also the condition of uniform potential vorticity by eq. (3); the resultant broadening of the jet is shown schematically in fig. 3. The potential vorticity field, determined from an analysis of particle streak photographs, is found to be fairly uniform over a wide radial region of the annulus, as plate I illustrates. The numerical simulations [4] indicate that this quasi-uniform potential vorticity is essential to the stability of vortices in our system.

The jet is turbulent for sufficiently large forcing flux  $F$ . Fig. 4 illustrates the fluctuations in the velocity for  $F = 185 \text{ cm}^3/\text{s}$ , which is in the middle of the range studied,  $15 < F < 370 \text{ cm}^3/\text{s}$ . Velocity values were determined by digitizing photographs

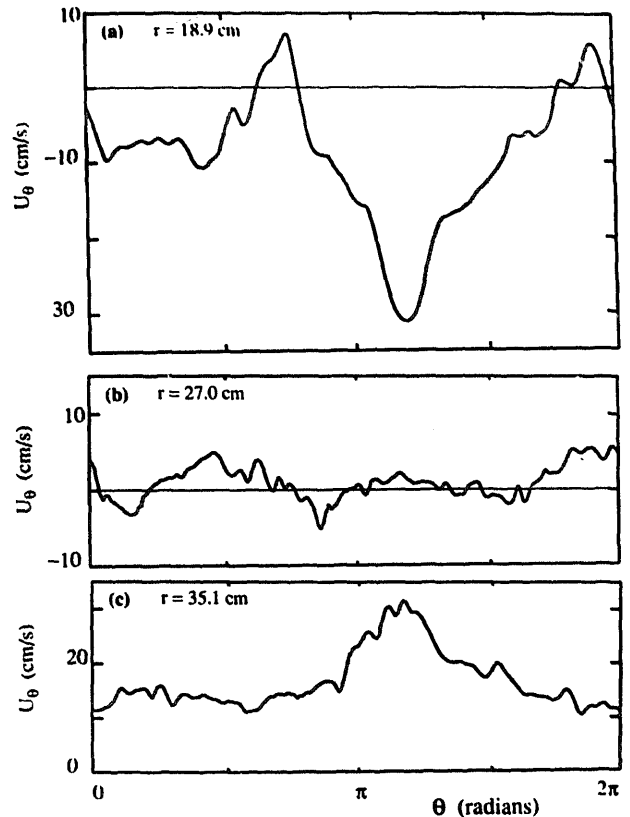


Fig. 4. The velocity fluctuations in the turbulent shear flow are illustrated in these graphs of the instantaneous azimuthal component of the velocity as a function of  $\theta$  at three different radii: (a)  $r = 1/4$  gap, (b)  $r = 1/2$  gap, which is the radial position of the vortex center, and (c)  $r = 3/4$  gap. ( $\Omega = 25.1 \text{ rad/s}$ ,  $F = 185 \text{ cm}^3/\text{s}$ ,  $Ro = 0.046$ ,  $Re = 47000$ .)

of particle streaks obtained from short time exposures of the flow [6]; the entire velocity field was then obtained by fitting the data with cubic splines. The velocity in fig. 4 is given with respect to a frame of reference in which the average velocity is zero near the mid-radius of the annulus. The strong peaks in fig. 4(a) and (c) are due to the presence of a large vortex (see below).

The average angular momentum of the jet,  $M = \rho \int r U(r) h_0 dA$ , is determined by a balance of the torque produced by the action of the Coriolis force on the radially pumped fluid and the torque produced by Ekman friction from the boundary layers at the upper and the lower surfaces of the tank ( $\rho$  is the density and  $U(r)$  is the azimuthally averaged component of the velocity). If the flow

were truly quasi-geostrophic, then

$$dM/dt = \rho \int 2\pi f(r) dr - M/\tau \quad (4)$$

should be zero. Here  $f(r)$  is the forcing function, roughly equal to  $\Omega Fr/\pi$ , and  $\tau = h_0/2(\nu\Omega)^{1/2}$  is the characteristic viscous decay time of quasi-geostrophic flow ( $\nu$  is the kinematic viscosity). We find that  $dM/dt$  is small, typically only about 4% of  $M/\tau$ . Further evidence that the flow is nearly geostrophic is provided by the particle streak photographs such as those in fig. 6, which will be discussed in detail later; particles at the same  $r$  and  $\theta$  but different vertical positions generally produce parallel streaks; the apparent crossing of some streaks is due to parallax in the optical system.

The observed flow patterns are not appreciably changed when some of the ports are closed, if the same total flow rate is maintained. This indicates that the dynamics is controlled not by the detailed geometry of the forcing but by inertial effects.

We present our results as a function of Reynolds number,  $Re = UL/\nu$ , and Rossby number,  $Ro = U/2\Omega L$ , where  $U$  is the velocity scale and  $L$  the length scale of the jet. Using results for  $U$  and  $L$  for marginally stable westward jet [6], we have  $Re = (d/4\pi\langle r \rangle \nu^{3/2})\Omega^{1/2}F$  and  $Ro = (9s^2d/16\pi\nu^{1/2}h_0^2\langle r \rangle)^{1/3}\Omega^{-1/6}F^{1/3}$ , where  $d$  is the radial separation of the ports and  $\langle r \rangle$  is the mean radius of the jet.

### 3. Results

#### 3.1. Single vortex regime

Over a wide range of parameters we find that a single stable cyclonic vortex forms in the cyclonic shear zone of the jet (see plate II) [5]; additional vortices continually form, but they rapidly merge with the primary vortex, as will be described in section 3.4. The vortex is an isolated structure, largely separate from the surrounding fluid flow.

When dye is injected *away* from a vortex and the Ekman layers, it mixes quickly throughout the turbulent fluid, but it does not penetrate into the vortex core, leaving the vortex to be seen as a bright spot (see plate II). Similarly, when dye is injected *directly into* a vortex, it remains in the vortex and does not quickly mix with the surrounding flow. The Ekman pumping leads to a weak downwelling within the upper half of a cyclonic vortex, a weak upwelling in the lower half, and a return vertical flow of the opposite sign outside the vortex. This pumping pulls clear fluid from the boundary layer into the vortex, diluting the dye in the vortex column; hence, a vortex that spontaneously forms in an initially uniformly dyed fluid becomes visible as a bright region. The magnitude of the vertical velocity from this pumping is  $w \approx Uh_0(\nu/2\Omega L^2)^{1/2}/L$ . For a vortex column of volume  $\pi L^2 h_0$ , the time required for the pumping to replace the fluid in the vortex is roughly 100 s for typical parameter values in the experiment ( $U = 20$  cm/s,  $L = 5$  cm,  $\nu = 0.01$  cm<sup>2</sup>/s,  $\Omega = 20$  rad/s).

Mixing between a vortex and the background flow can be inhibited by a potential vorticity gradient around a vortex: when a parcel of fluid crosses the gradient it undergoes a rapid change in vorticity, resulting in the advection of the surrounding fluid that then acts on the original parcel to restore it to its final position. In general, this is the restoring mechanism for Rossby waves. The potential vorticity gradient around a vortex can be seen in plate I(b). We have observed in other experiments using the same apparatus that strong potential vorticity gradients act to inhibit mixing [6, 7].

Vortices observed in a shear flow in some previous experiments were interpreted to be Rossby solitons [10]. However, the vortices observed in our turbulent shear flow *cannot* be Rossby waves – the observed vortices, unlike Rossby solitons, do not propagate with respect to the background flow. The stationarity of a vortex center with respect to the background flow is illustrated by the data in fig. 4(b): the average azimuthal

velocity with respect to the background velocity at the radial position of the vortex center is zero. The absence of propagation is related to the uniform potential vorticity of the background flow (as e.g., in plate I); a flow with uniform potential vorticity cannot support Rossby waves [7, 8].

We find that a single dominant vortex always forms for sufficiently rapid rotation rates ( $\geq \sim 2$  Hz) and pumping rates ( $\geq \sim 100$  cm<sup>3</sup>/s). The single vortex regime extends to the limits of our parameter ranges,  $\Omega = 25$  rad/s and  $F = 370$  cm<sup>3</sup>/s. Moreover, given the insensitivity to the details of the forcing, it appears that the formation of a single vortex is a robust phenomenon in quasi-geostrophic turbulent shear flows.

### 3.2. Multiple vortices

The single vortex state dominates most of the parameter region studied, but for sufficiently small Reynolds number and Rossby number multiple vortices are observed, as indicated in the regime diagram in fig. 5. Five weak vortices are observed at  $Re = 2200$  and  $Ro = 0.033$ . When the Reynolds number is increased, a critical value is reached at which there is a transition to four vortices. Further increases in pumping rate lead to transitions to three and then to two and finally to one vortex (see the phase diagram in [5]). Each regime with a

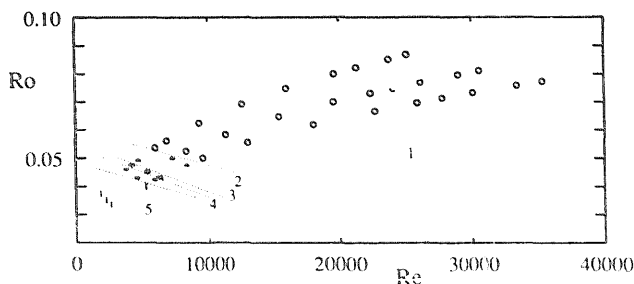


Fig. 5. The number of stable vortices rapidly decreases with increasing Reynolds and Rossby numbers until the single vortex regime is reached. Regimes with different numbers of vortices are indicated with different symbols and are separated by dotted lines. There is some hysteresis, so the locations of the transition boundaries would be different for decreasing Reynolds and Rossby numbers.

multiple number of vortices exists only over a narrow range in  $Re$  and  $Ro$ . The velocity field in these regimes exhibits some fluctuation, but, in contrast to the single vortex regime, it is not strongly turbulent. Experiments are planned with hot-film probe measurements of velocity time series to determine if the fluctuations in the multiple vortex regimes are describable by low-dimensional multiperiodic or chaotic phase space attractors, as has been found in some previous experiments on other simple geophysical flows [11].

We cannot predict quantitatively how the spacing between vortices in the multiple vortex states depends on the control parameters and geometry, but it is clear that the spacing and the vortex size are determined in part by the width of the jet and by the relevance of friction to the dynamics [5]. For example, the region of uniform potential vorticity is narrower for a three-vortex state in plate III than for the single vortex state in plate I(b). Increasing vortex size permits vortices to interact, resulting ultimately in a merger between two vortices. For a given jet width, maintained by changing both the rotation rate and pumping flux, the spacing between vortices increases as the Ekman friction is decreased. Multiple vortex states are found for Ekman times comparable to vortex turnover times, while a single vortex is obtained in flows less influenced by friction.

### 3.3. Turbulence

The irregularity of the flow in the single vortex regime is illustrated by the plots of vorticity and potential vorticity shown in plate I and by the velocity graphs in fig. 4. The energy spectrum computed from data for the velocity field has a steep dependence on wavenumber, but our resolution is insufficient to determine the power law. Two-dimensional homogeneous turbulence without beta effect (on an  $f$ -plane) is described by a  $k^{-3}$  power law, which can be altered by forcing [12] and the beta effect [13], and by coherent structures that destroy homogeneity. The presence of the mean flow may also influence the character

of the turbulence. Our experiment, which involves all of these effects, seems far from the domain typically studied in geophysical turbulence.

Observations of the dye clearly show continuous complex deformation of a vortex, probably due to interactions with turbulence and small eddies. Vortex material is sometimes greatly twisted by strong interactions (such as a merging), and potential vorticity is stretched over a large “longitude” but quickly recoalesces into a roughly elliptical shape; similar behavior was found in the

simulation by Marcus [4, 14]. His work implies that an arbitrary distribution of excess potential vorticity a few times greater than the background vorticity on a uniform potential vorticity shear flow will rapidly coalesce into a single vortex, if the excess vorticity has the same sign as the shear. The continuous deformations are reminiscent of the deformation associated with vortex merging, indicating that the vortex may be absorbing eddies too small for us to observe. There may also be a direct effect of the forcing: sinks produce cyclonic

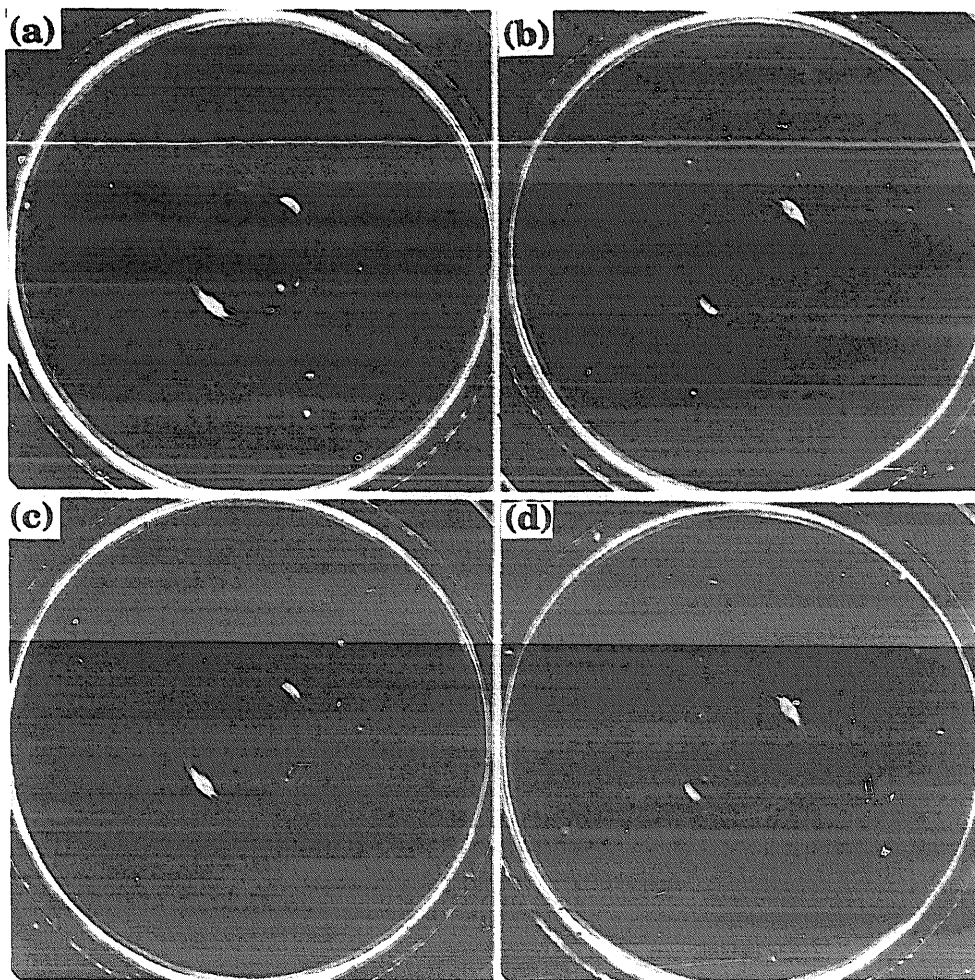
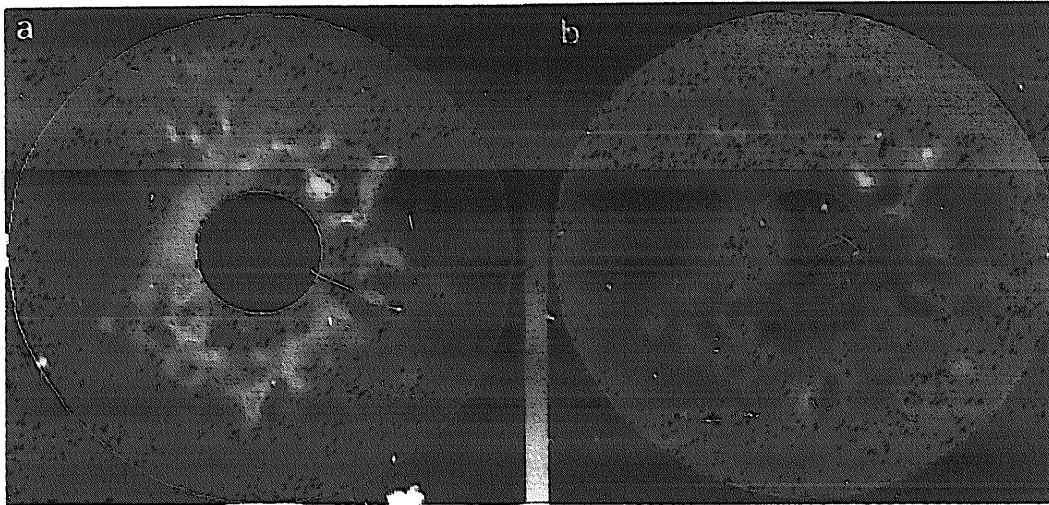
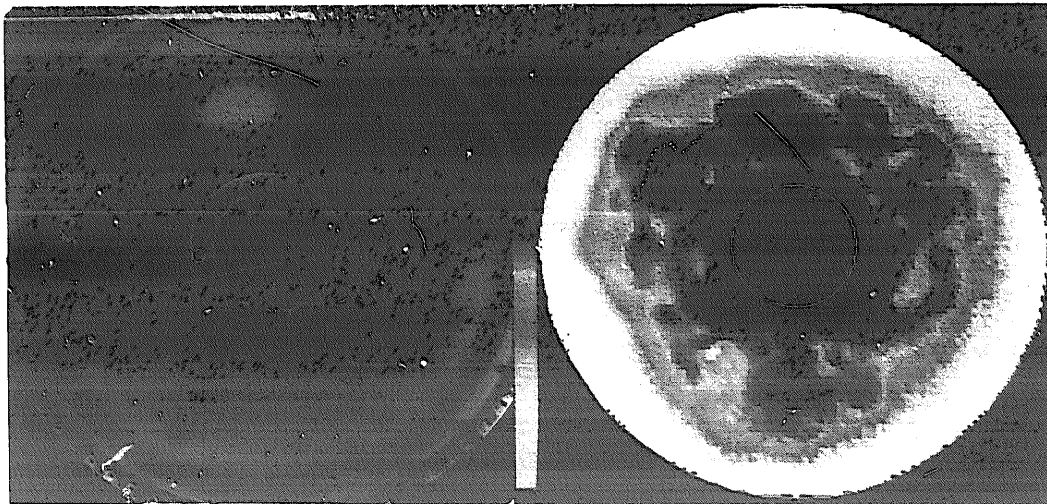


Fig. 6. The merging of two vortices is visualized in this time sequence of photographs of particle streaks. (a)  $t = 0$ : a state with two vortices, a single stable vortex and a secondary vortex on the lower left; the secondary vortex has existed long enough to grow appreciably in size. (b)  $t = 4$  s: the vortices are advected toward one another by the shear flow. (c)  $t = 8$  s: the velocity fields of the two vortices are beginning to interact and the merging process is underway. Visualization of the flow with dye [5, 6] reveals a wrapping around the vortices in this stage of the merging process. (d)  $t = 12$  s: the two vortices have merged into a single vortex. Once the vortices begin to interact, the merging quickly occurs. ( $\Omega = 25.1$  rad/s,  $F = 137$  cm<sup>3</sup>/s, exposure time 0.25 s; the camera rotation frequency was 24.4 rad/s, which is approximately the rotation frequency of the vortices around the annulus,  $Ro = 0.042$ ,  $Re = 35000$ .)



**Plate I**



**Plate II**

**Plate III**

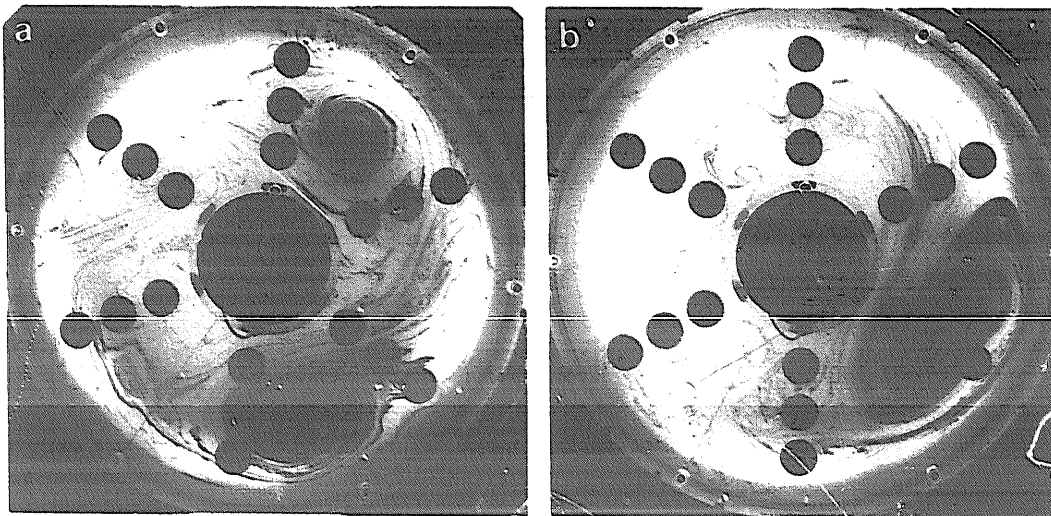


**Plate IV**



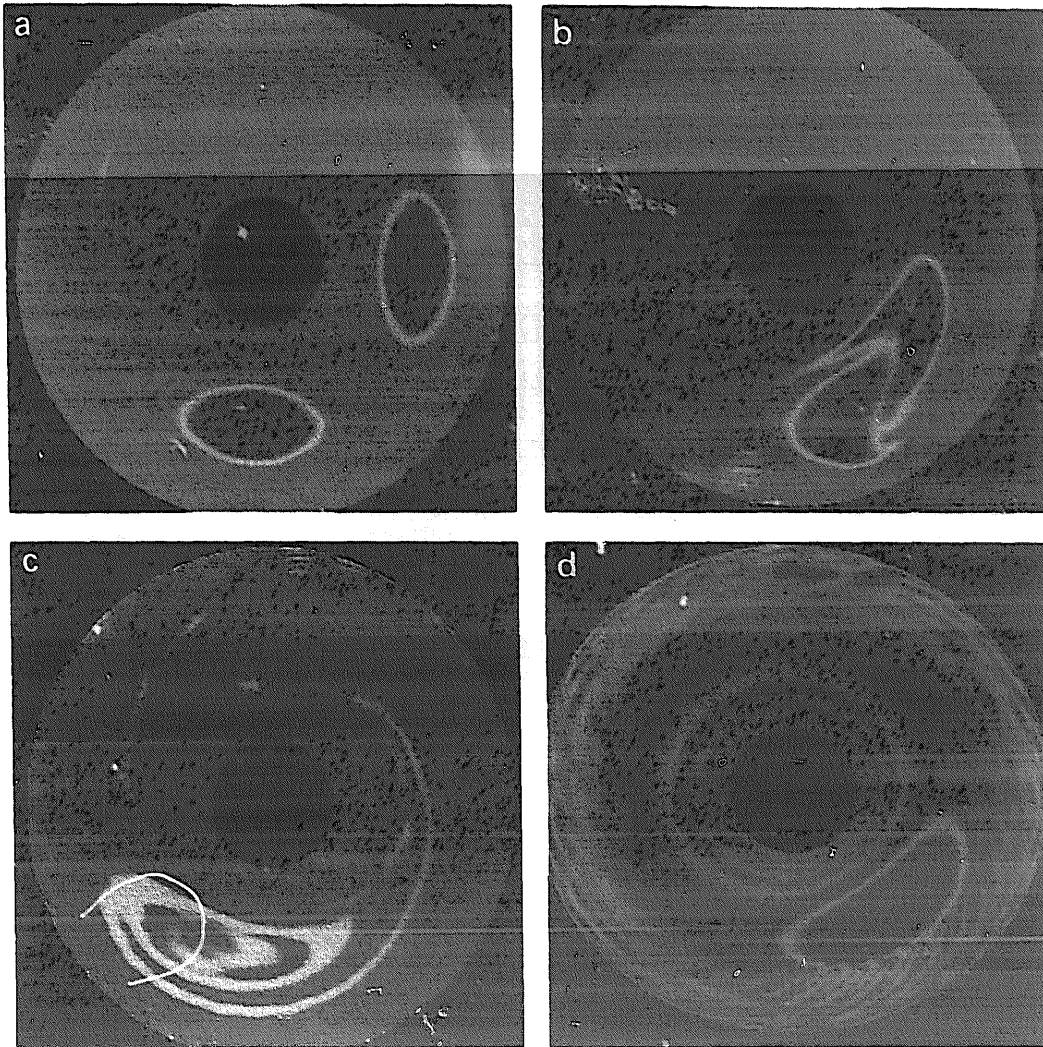


Plate V

**Plate I.** (a) The vorticity distribution indicates the flow is turbulent. The turbulence probably continues to length scales smaller than our present digital imaging system can resolve (about 1 cm). The color bar indicates the scaling of vorticity in the range from  $-10.9$  rad/s (white) to  $9.95$  rad/s (red). (b) The potential vorticity is fairly uniform over a wide region of the annulus. The color bar indicates the scaling of potential vorticity in the range from  $-15.2$  rad/s (white) to  $3.52$  rad/s (red). ( $Ro=0.12$ ,  $Re=18700$ .)

**Plate II.** A single vortex spontaneously forms in a turbulent shear flow in the rapidly rotating annulus. Dye injected away from the vortex rapidly mixes in the turbulent region but is inhibited from penetrating the vortex core. ( $Ro=0.12$ ,  $Re=13100$ .)

**Plate III.** The potential vorticity for a state with three stable vortices is uniform over a smaller region of the annulus than in the regime with a single vortex; compare plate I (b). The color bar indicates the range of potential vorticity from  $-8.5$  rad/s (white) to  $-0.1$  rad/s (blue). ( $Ro=0.093$ ,  $Re=5900$ .)

**Plate IV.** The ejection of potential vorticity is rendered visible by dye, a passive scalar. (a) Before the merger there is little dye outside the vortices. (b) After the merger there are large tongues of dye outside the vortex; the ejected potential vorticity feeds the background flow. ( $Ro=0.14$ ,  $Re=21900$ .)

**Plate V.** The merging sequence observed in a numerical simulation [4] is remarkably similar to that observed in the experiments (compare fig. 7) and to that on Jupiter (compare fig. 9). (a)  $t=0.0$ . Two vortices are superposed on an axisymmetric, azimuthal flow with uniform potential vorticity. The two vortices and the background shear flow have the same sign of vorticity. (b)  $t=1.3$  (time is measured in vortex turnover times). The vortices have been advected toward one another by the shear flow, and they are beginning to merge. (c)  $t=2.6$ . The vortices have merged, but the potential vorticity within the spot is not yet uniform. Note the ejection of excess vorticity. (d)  $t=28$ . The merging process is complete. Color represents potential vorticity with low values in green and strong anticyclonic values in red.

vorticity, and when a cyclonic vortex passes over a sink, there is probably an interaction that helps maintain the vortex. It is, however, difficult to separate the effects of turbulence from the action of the ports.

In a numerical simulation of a single layer model of a terrestrial stratospheric polar vortex, Jukes and McIntyre [15] observed the spontaneous formation of a stable anticyclonic vortex in a well-mixed anticyclonic shear flow (near the polar vortex). They found the mixing outside the polar vortex occurred quickly and was related to a wave-breaking phenomenon. The polar vortex was found to be an essentially isolated structure surrounded by a strong potential vorticity gradient, in spite of the surrounding turbulence.

### 3.4. Merging

In the single vortex regime small vortices are continually being created by the action of the pumping. Anticyclonic vortices are unstable in the cyclonic shear and are rapidly destroyed (within one Ekman time), while cyclonic vortices merge with the large vortex, as figs. 6 and 7 illustrate. A secondary vortex generally merges with the primary vortex soon after it is formed. We can then clearly distinguish the primary vortex from a secondary one by their strengths and by their trajectories during merging – the primary vortex moves less than the secondary one around their “center of gravity”. A major merging event occurs roughly

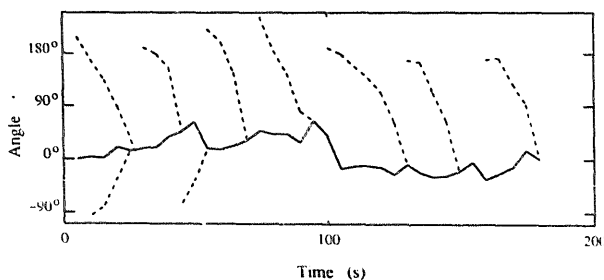


Fig. 7. Secondary vortices, whose trajectories are shown by dashed lines, repeatedly merge with the single primary vortex, whose trajectory is shown by the solid line. ( $\Omega = 25.1$  rad/s,  $F = 137$  cm<sup>2</sup>/s,  $Ro = 0.042$ ,  $Re = 35000$ ).

every Ekman spin-down time, which is the time necessary for a new vortex to be created. Most secondary vortices approach the primary vortex from the “west”, a few from the “east”. The latter mergings typically involve small vortices that have formed from material ejected during a previous merging. Sometimes two small vortices will first merge with one another before merging with the primary vortex. For intermediate forcing levels a new vortex generated at a position opposite in azimuth to the primary vortex can grow until it reaches a size comparable to the main vortex; however, a fluctuation will bring the vortices closer, leading to a rapid merger. For strong forcing, merging occurs before a secondary vortex can grow appreciably in size.

When two vortices merge, there is often a significant ejection of material in the form of long thin tongues, as plate IV illustrates. Dye, a passive scalar, is advected with the potential vorticity (over short times scales) and hence yields information on the potential vorticity dynamics. A vortex will grow through the merging process until it fills the zone of uniform potential vorticity; then when a merger occurs, dye is ejected outside of this zone and is quickly advected away, indicating an ejection of potential vorticity.

## 4. Discussion

### 4.1. Merging

We now compare the laboratory observations of merging with numerical simulations and with observations of Jupiter. In a numerical simulation of quasi-geostrophic flow of an inviscid fluid in an annulus, Marcus [4, 14] found that for a wide variety of initial conditions a large stable vortex formed in a flow with uniform potential vorticity (even with  $\beta = 0$ ) if the vortex had the same sign of vorticity as the background shear. Vortices of the opposite sign of vorticity were unstable and disintegrated. If the flow initially had two vortices of the same sign as the background shear, they

rapidly merged, as plate V illustrates. Potential vorticity was shed during these simulated mergers, creating a turbulent background flow of uniform potential vorticity. Marcus [14] suggested that for merging to occur there must be a transfer of energy (via shedding) to smaller scales, a process normally inhibited in geostrophic turbulence. The presence of small scale forcing in our experiment may be an important factor in allowing merging to occur.

No previous experiment has demonstrated merging of two free vortices in a quasi-geostrophic turbulent shear zone with a beta effect, yet this merging is an essential property of jovian vortices, as Mac Low and Ingersoll have discussed [2]. They studied all of the photographs taken by the voyager 2 spacecraft and found that there were 27 cases involving interactions of vortices; 24 of the interactions resulted in merging – an example is shown in fig. 8. The other three encounters were near misses. The merging of the Great Red Spot with a smaller vortex can be seen in the famous NASA “blue movie” made from Voyager 1 photographs. Merging of jovian vortices occurs within a few vortex turn-over times, and the ejection of excess material can be seen during a merging (e.g., see fig. 8), which suggests that vortex size is limited by the width of the zone.

#### 4.2. Radius of deformation

A major difference between our experiment and the planet Jupiter is our lack of significant vertical structure. In an atmosphere or ocean, which are stratified in density, hydrostatic forces can oppose vertical gradients of the geostrophic pressure, and the flow can be different at different vertical levels (i.e., the flow has a baroclinic part). To simplify the discussion we consider a model with two layers of constant density separated by a discontinuity. Different velocities in two adjacent layers induce a slope of the interface that can be calculated by writing the balance of pressure forces along a closed circuit, as represented in fig. 9. The

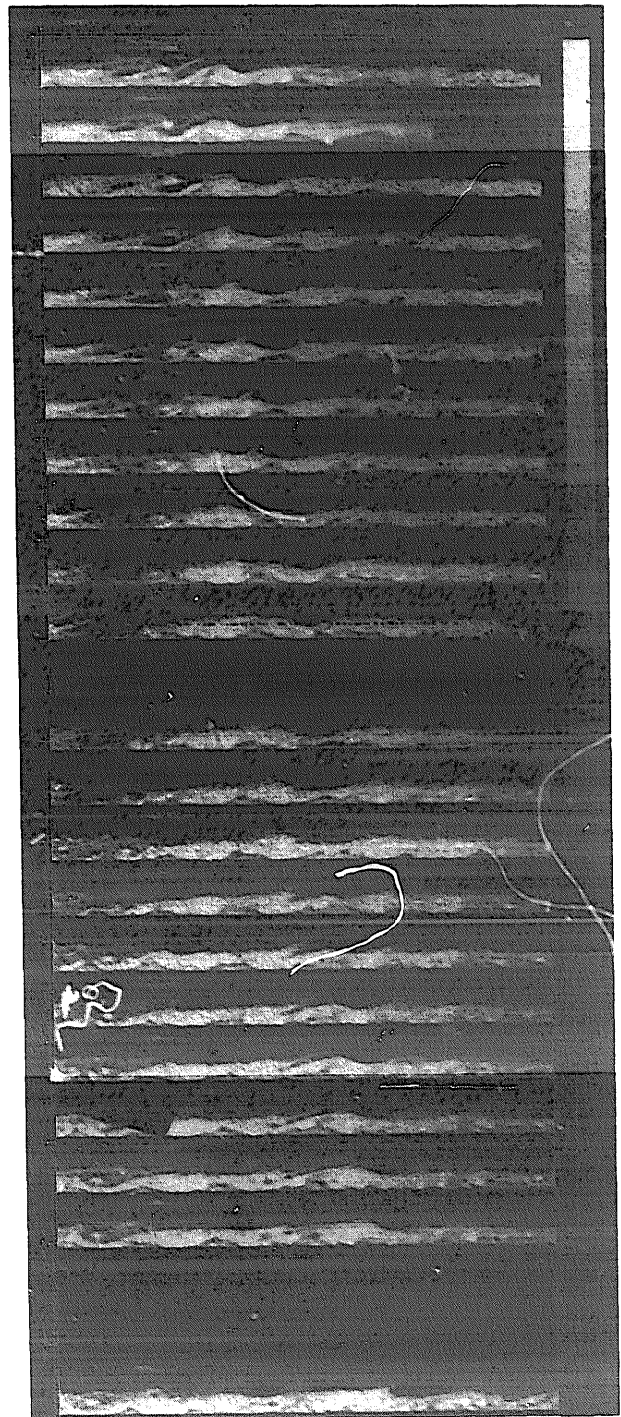


Fig. 8. The merging of two vortices in the jovian atmosphere is beautifully illustrated by these Voyager 2 photographs compiled by MacLow and Ingersoll [2]. The 25 strips show a zone at  $34^\circ$  N for 25 successive rotations of Jupiter (one rotation is 9 h 55 min). Each strip covers an area approximately  $70\,000\text{ km} \times 7\,000\text{ km}$ . Note the material streaming away from the spot after the interaction.

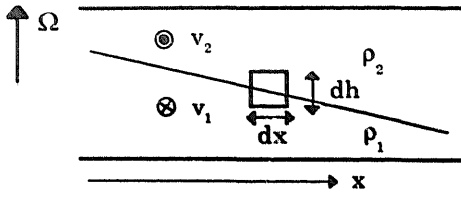


Fig. 9. Two geostrophic layers of densities  $\rho_1$  and  $\rho_2$  have velocities  $V_1$  and  $V_2$  into and out of the paper respectively, causing a deformation of the interface due to the geostrophic pressure. Here the simple case of uniform velocity in each layer results in a uniform deformation of the interface.

contribution of the two horizontal sections is obtained from the geostrophic balance, while the contribution of the two vertical sections is obtained from the hydrostatic balance (assuming small horizontal displacement  $dx$  and vertical displacement  $dh$ ). The pressure balance along the infinitesimal circuit yields

$$(\rho_1 - \rho_2)g dh = 2\Omega(\rho_1 V_1 - \rho_2 V_2) dx, \quad (5)$$

where the subscripts 1 and 2 are for the lower and upper layers respectively,  $g$  is the acceleration of gravity, and  $V_1$  and  $V_2$  are the horizontal velocity components perpendicular to the displacement  $dx$  (the  $V_i$  do not depend on the vertical coordinate). Eq. (5) generalizes to the thermal wind equation in a model with continuous stratification [8]. With the differential of the stream function given by  $d\psi_i = V_i dx$ , integration of (5) yields

$$h(x, y) = h_0 + (2\Omega / (f_1 - \rho_2)g)(\rho_1\psi_1 - \rho_2\psi_2). \quad (6)$$

With negligible friction and forcing, the potential vorticity is conserved for a fluid parcel in each layer. For small deformations, the thickness  $h_i$  of each layer can be expanded around a mean value  $h_{i,0}$ , and the quasi-geostrophic expression for the potential vorticity is then obtained. We consider two layers limited at the upper and lower levels by rigid boundaries (or boundaries with a large density step), and assume that the difference in density  $|\rho_2 - \rho_1|$  is small compared to the mean density  $\rho_0$ . The potential vorticity in each layer is

then

$$q_1 = \omega_1 + \beta y - (\psi_1 - \psi_2)/R_1, \quad (7a)$$

$$q_2 = \omega_2 + \beta y - (\psi_2 - \psi_1)/R_2, \quad (7b)$$

where  $R_i = (1/2\Omega)(h_{i,0}g|\rho_2 - \rho_1|/\rho_0)^{1/2}$  is the Rossby deformation radius of the  $i$ th layer.

The effect of deformation on the dynamics is only important for horizontal eddies of size equal to or greater than the radius of deformation. On smaller scales the dynamics are two-dimensional. In our apparatus the fluid has no free surface, so the deformation radius is effectively infinite; therefore, our system models dynamics on scales small compared to the deformation radius. However, except for a vortex screening effect, the dynamics for a system with a finite deformation radius probably should not differ significantly from that of a system with an infinite deformation radius. The screening effect arises from the self-interaction term, which changes the Laplacian operator that relates the vorticity to the stream function,

$$\omega = \nabla^2 \psi, \quad (8)$$

into the operator  $(\nabla^2 + 1/R_i)$  [8]: thus a vorticity patch in the  $i$ th layer will generate a velocity field confined to a scale  $R_i$ , rather than an infinite vortex with a  $1/r$  profile as in the barotropic case. In particular, the mechanism of propagation of Rossby waves is the same for the two cases, though the speed of propagation drops exponentially for wavelengths larger than the radius of deformation.

If the lower layer is relatively thick, its radius of deformation is very large and, as expected because of the large inertia, its dynamics will not be modified by the upper layer. The effect of a thick lower layer on a steady upper layer is equivalent to a modification of the beta effect by bottom topography. Fluctuations in the lower flow will act as unsteady sources and sinks of vorticity for the thin upper layer. Such a model with two layers of very different depth seems to be appropriate for the jovian flows [16].

In the jovian atmosphere the radius of deformation is estimated to be 1000–5000 km [4, 17]. The largest spots are much larger than the deformation radius and the small spots are much smaller than this radius; however, the basic properties of the spots – indeed, their very existence – do not seem to depend on the deformation length scale. Our laboratory vortices, which are small compared to the (infinite) radius of deformation in the annulus, have stability and merging properties similar to the jovian vortices. Moreover, simulations show that the stability and the merging properties of spots are *not* strongly influenced by their size [4, 14]. Thus experiments, simulations, and observations of jovian spots indicate that the basic dynamics of vortex formation may be understood in terms of a scale-independent model based on inertial effects.

#### 4.3. Vorticity profile; beta effect

Our laboratory vortices have a vorticity maximum at the center, while the vorticity structure of the Great Red Spot and the White Ovals have annular profiles (the vorticity structure of small jovian spots has not yet been determined) [18, 19]. Marcus's numerical simulations [4] show that free surface deformation results in an annular structure of vorticity for vortices whose radius of deformation is small compared to the vortex size. In our laboratory model we do not have a free surface and the vorticity lines are unable to contract due to deformation effects, leaving the vorticity peak in the center of our vortices unchanged.

The interpretation of jovian vortices as Rossby solitons has been investigated both experimentally [10] and numerically [20]. Rossby solitons have a Gaussian distribution of vorticity peaking at the center, a distribution that is apparently independent of the relative size of the deformation radius. While this vorticity distribution is contrary to that observed for large jovian vortices, the soliton model does give a possible explanation for the rareness of cyclonic vortices on Jupiter: a dynamical asymmetry between cyclonic and anticyclonic

vorticity arises when  $\beta \neq 0$ . Anticyclones would be stable while cyclones would be unstable for  $\beta > 0$ . However, the model ignores motion in the deep lower atmosphere of Jupiter that can act as sources and sinks of potential vorticity, effectively altering (even eliminating) the beta effect in the thin upper layer. Marcus's simulations and our experiments show that well-mixed turbulent flows such as those on Jupiter tend to achieve a fairly uniform potential vorticity, significantly decreasing the beta effect.

Although the vorticity profile of large vortices can be deduced from Voyager data, the determination of the beta effect is not straightforward. In a model with a barotropic atmospheric layer floating on a deep denser underlying fluid, pressure differences due to differential rotation in the lower layer would create effects like a sloping bottom. The total beta effect would then result both from this slope and from the planetary curvature. One way to measure this slope is to follow the vorticity of a fluid particle that changes latitude, assuming that  $\omega/h$  is constant. Dowling and Ingersoll [19, 21] did this by following small clouds above the Red Spot and White Ovals, and they found that the bottom topography is zonally dependent, influencing the upper layer. From this they could obtain an approximate potential vorticity for the zonal flow surrounding the jovian vortices. They found the potential vorticity of the zonal flow under the White Oval BC was uniform to within the uncertainty (about 10%) but the potential vorticity under the GRS varied by as much as 50%. A better understanding of the nature of the total beta effect on Jupiter and its influence on the formation of persistent vortices awaits more detailed knowledge of the jovian atmosphere.

#### 4.4. Vortex formation and multiple vortices

Voyager photographs reveal jovian vortices over a wide range of latitudes, as can be seen in figs. 1 and 10. The chains of regularly spaced vortices at the higher latitudes are evocative of the vortex



Fig. 10. A composite picture of Voyager photographs of Jupiter's southern polar regions, which contains many vortices, including the Great Red Spot ( $22.5^\circ$  S). White Ovals and a chain of vortices at  $41^\circ$  S. (Photograph from Jet Propulsion Laboratory, NASA.)

chains observed in laboratory flows, but the history and dynamics of the jovian vortex chains are not known well enough to make direct comparisons with vortex chains found in the laboratory. However, some similarities are apparent. Small jovian vortices are located in thin shear zones: the zone containing multiple vortices at  $41^\circ$  S is roughly half as wide as the zone containing the GRS. Williams and Wilson [20] have also found in their numerical simulations of Rossby vortices that a narrow shear zone often leads to a state with many vortices. The ellipticity of the anticyclonic jovian vortices decreases from about two for large vortices to unity for small vortices [2], while the cyclonic barges are highly elliptical.

Jovian vortices are well separated from their surroundings. Close-up photographs of the Red Spot and the White Ovals show a sharp demarcation between a vortex and the turbulent jets (fig. 1(b)). In fact, most vortices are visible because they are a different color (implying a different composition) than their surroundings, remaining so for days or years. The present day White Ovals were first reported around 1938. However, there

were large white vortices present at the same latitude in 1918 that were never reported to disappear, but were obscured by a general brightening of the atmospheric material. In 1938 three dark regions spread longitudinally at this latitude, leaving the large White Ovals [22]. It is possible that the Ovals were the previously observed vortices [23], and the surrounding dark clouds again rendered them visible. Material injected into the upper atmosphere might be inhibited from mixing with the vortices if they were surrounded by strong potential vorticity gradients, as found in our experiments (see section 3.1). Dowling and Ingersoll [21] have found such a gradient around the GRS which may explain why the jovian vortices can maintain an isolated existence amidst turbulence for long periods of time.

#### 4.5. *Other experiments*

Previous laboratory models for the Red Spot used rotating fluid systems, driven in a different manner from ours. A more significant difference is probably the smaller dissipation in our experiments.

Antipov et al. and Nezlin [10] have explored the stability of a barotropic shear flow produced by a differential rotation of axisymmetric bands in the bottom of a parabolic tank. Vortices of both signs were observed to arise from an instability of the shear flow; only anticyclones were stable in the widest shear. Although their experiment is related to our own, achieving a single long-lived vortex in a shear zone of the same sign, there are significant differences between their work and ours. They achieve a single vortex only in a narrow parameter range, corresponding to a wide zone with a large shear. Their flow had a free surface, and the fluid depth in a vortex was typically 40% greater than the background flow; this seems to violate the geostrophic approximation they used in interpreting their results. Although they observed merging of vortices, it was reported only for circumstances inappropriate for Jupiter, i.e., when there was no shear or when there was a transition between

stable multiple vortex states. Antipov et al. did not observe a regime in which a single dominant vortex repeatedly absorbed all others in a shear flow. The Ekman time scale was comparable to the vortex turnover time, while in our experiment the Ekman time was an order of magnitude longer than the turnover time. In some of their photographs the flow appears to be turbulent around the vortex, implying a mixing of potential vorticity; however, this issue and its implications for vortex stability were not discussed.

An experiment by Niino and Misawa [25] examined the dynamics of vortices in a barotropic jet. These experiments were not designed to model jovian dynamics, but the results bear some resemblance to those found in other experiments discussed here. Theoretical considerations were used to demonstrate that instability arises in a geostrophic shear flow driven by axisymmetric differential rotation; the observed vortices were interpreted as arising from this instability. The number of vortices decreased with increased forcing. Merging in these experiments occurred only at the transition between multiple-vortex states. A single vortex regime with repeated merging was not observed. Turbulence was not discussed, but the photographs suggest that the flow was sometimes irregular.

The heated annulus of Read and Hide [26] produces long-lived vortices via a baroclinic instability. In one series of experiments they studied flow in a rotating annulus heated internally and cooled on the sides. In a narrow range of parameters, a single large anticyclonic vortex formed in a laminar shear flow, shadowed by a smaller cyclonic vortex. Chains of these vortex pairs were also found for slightly different parameter values. They suggested that the Red Spot is a thermally driven entity, though recent estimates of Jupiter indicate that thermal effects are weak compared to inertial ones [16]. Since their flow was baroclinic (hence strongly 3-dimensional), it is difficult to make direct comparisons between their experiment and ours, despite some superficial similarities.

#### 4.6. Concluding remarks

The robust vortices found for a variety of conditions in our experiments and in the numerical simulations of Marcus have many properties in common with jovian spots. The vortices are of the same sign as the background shear; the vorticity is typically 2–4 times that of the background shear; the length to width ratio is about two for the larger vortices; the vortices are located near the maximum of the shear and are advected at the corresponding velocity of the background flow (that is, they do not propagate with respect to the surrounding fluid); and finally, the process of vortex merging observed in the laboratory and in the simulations is very similar to that on Jupiter.

#### Acknowledgements

This work is supported by the Office of Naval Research Nonlinear Dynamics Program. J.S. is supported in part by the Centre National de la Recherche. The collaboration between the Texas and French groups is supported by a NATO travel grant.

#### References

- [1] R. Hooke, *Phil. Trans. Roy. Soc.* 1 (1666) A2.
- [2] M.M. MacLow and A.P. Ingersoll, *Icarus* 65 (1986) 353–369.
- [3] A.P. Ingersoll, R.F. Beebe, J.L. Mitchell, G.W. Garneau, G.M. Yagi and J. Muller, *J. Geophys. Res.* 86 (1981) 8733–8743.
- [4] P. Marcus, *Nature* 331 (1988) 693–696.
- [5] J. Sommeria, S.D. Meyers and H.L. Swinney, *Nature* 331 (1988) 689–693.
- [6] J. Sommeria, S.D. Meyers and H.L. Swinney, to appear in: *Nonlinear Topics in Ocean Physics*, A. Osborne, ed. (North-Holland, Amsterdam, 1989).
- [7] J. Sommeria, S.D. Meyers and H.L. Swinney, *Nature* 337 (1988) 58–61.
- [8] J. Pedlosky, *Geophysical Fluid Dynamics*, 2nd edition (Springer, New York, 1987).
- [9] H.L. Kuo, *J. Meteorology* 6 (1949) 105–122.
- [10] S.V. Antipov, M. Nezlin, E. Snezhkin and A. Trubnikov, *JETP Sov. Phys.* 55 (1982) 85–95.

- M.V. Nezlin, *Sov. Phy. Usp.* 29 (1986) 807–842.
- [11] J. Guckenheimer and G. Buzyman, *Phys. Rev. Lett.* 51 (1983) 1438–1451.  
J.E. Hart, *Physica D* 20 (1986) 350–362.
- [12] R. Salmon, in: *Topics in Ocean Physics*, A. Osborne and P. Malanotte Rizzoli, eds. (North-Holland, Amsterdam, 1982), pp. 30–78.
- [13] P.B. Rhines, *J. Fluid Mech.* 69 (1975) 417–443.
- [14] P. Marcus, *J. Fluid Mech.* (1989), to appear.
- [15] M. Jukes and M.E. McIntyre, *Nature* (1987) 590–596.
- [16] J. Yano, *J. Met. Soc. Japan* 65 (1987) 313–326.
- [17] A.P. Ingersoll and P.G. Coung, *J. Atm. Sci.* 38 (1981) 2067–2076.  
G.P. Williams, *Adv. Geophys.* 15 (1985) 381–427.
- [18] J.L. Mitchell, R.F. Beebe, A.P. Ingersoll and G.W. Gareau, *Nature* 280 (1981) 776–778.
- [19] T.E. Dowling and A.P. Ingersoll, *J. Atm. Sci.* 45 (1988) 1380–1396.
- [20] G. Williams and R.J. Wilson, *J. Atm. Sci.* 45 (1988) 207–241.
- [21] T.E. Dowling and A.P. Ingersoll, *J. Atm. Sci.* (1988), to appear.
- [22] R.F. Beebe and L.A. Youngblood, *Nature* 280 (1979) 771–775.
- [23] E.J. Reese, *Icarus* 17 (1972) 704–706.
- [24] F.M. Flasar, B.J. Conrath, J.A. Pirraglia, P.C. Clark, R.G. French, and P.J. Gierasch, *J. Geophys. Res.* 86 (1981) 8759–8767.
- [25] H. Niino and N. Misawa, *J. Atm. Sci.* 41 (1984) 1992–2011.  
See also M. Dunst, *J. Fluid Mech.* 60 (1973) 391–400.
- [26] P.L. Read and R. Hide, *Nature* 308 (1984) 45–48.  
P.L. Read, *Icarus* 65 (1986) 304–334.